
Article:
Ascolani, G., Skerry, T.M. orcid.org/0000-0003-1319-5575, Lacroix, D. orcid.org/0000-0002-5482-6006 et al. (2 more authors) (2021) Analysis of mechanotransduction dynamics during combined mechanical stimulation and modulation of the extracellular-regulated kinase cascade uncovers hidden information within the signalling noise. Interface Focus, 11 (1). 20190136. ISSN 2042-8901

https://doi.org/10.1098/rsfs.2019.0136

Analysis of Mechanotransduction Dynamics During Combined Mechanical Stimulation And Modulation of ERK Cascade Uncovers Hidden Information Within The Signalling Noise

Gianluca Ascolani[1,2], Timothy M. Skerry[1], Damien Lacroix[2,3], Enrico Dall'Ara[1,2] and Aban Shuaib[1,2] *

* Correspondence: aban.shuaib@sheffield.ac.uk, Department of Oncology & Metabolism, University of Sheffield, Sheffield, UK

Full list of author information is available at the end of the article

Abstract

Osteoporosis is a bone disease characterised by brittle bone and increased fracture incidence. With aging societies worldwide, the disease presents a high burden on health systems. Furthermore, there are limited treatments for osteoporosis with just two FDA approved anabolic pharmacological agents. Healthy bones are believed to be maintained via an intricate relationship between dual biochemical-mechanical (bio-mechanical) stimulations. It is widely considered that osteoporosis emerges due to disturbances of said relationship. Mechanotransduction process is key to this balance, and disruption of its dynamics in bone cells play a role in osteoporosis development. Nonetheless, the exact details and mechanisms that drive and secure the health of bones are still elusive at the cellular and molecular scales. This study examined the dual modulation of mechanical stimulation, and mechanotransduction activation dynamics in an osteoblast (OB). The aim was to find patterns of mechanotransduction dynamics demonstrating a significant change that can be mapped to alteration in OB responses, specifically at the level of gene expression and osteogenic markers such as alkaline phosphatase (ALP). This was achieved using a 3D hybrid-multiscale computational model simulating mechanotransduction in OB and its interaction with the extracellular matrix (ECM), combined with a numerical analytical technique. The model and the analysis method predict that within the noise of mechanotransduction, due to modulation of the bio-mechanical stimulus, and consequent gene expression, there are unique events that provide signatures for a shift in the system's dynamics. Furthermore, the study uncovered molecular interactions that can be potential drug targets.

Keywords: osteoblast; osteoporosis; dual biomechanical signalling; mechanotransduction; multiscale model; agent-based modelling, molecular network; fluctuations; subordination theory; directing process; waiting time distribution

Abbreviations

ABM: Agent-based model,

ACS: Activation Cycle Switch,

BR: Bone remodelling,

ECM: Extracellular matrix,

EGF = epidermal growth factor,

ERK: Extracellular signal-regulated kinase,

iPTH= PTH analogue,

Mech-ABM: hybrid mechanical-ABM model,

MEK: MAPK/Erk kinase,

pERK =phosphorylated ERK,

PTH = Parathyroid hormone

PTHR = PTH receptor

Raf: Rapidly Accelerated Fibrosarcoma,

OB: Osteoblast,

OCy: Osteocyte,

OC = osteoclast,

SIP = signal interim period,

WTD: Waiting Time Distribution

Background

Osteoporosis as a skeletal disease presents a burden to health systems worldwide while the average life expectancy increases. In the UK, it has been predicted that it will cost the NHS over £2.2 billion per year in 2025, with the expected cost rising annually[1]. The disease causes changes in bone architecture, a reduction in its optimum mechanical properties and thus an increased likelihood of fractures [2]. The disease provides a multiscale challenge as bone mechanical properties and strength, at the tissue level, are a product of intercellular and intracellular interactions. The building unit of bones is the bone-remodelling unit (BRU) consisting of osteocytes (OCy), osteoblasts (OB) osteoclasts (OC) and the bone extracellular matrix (ECM) [3]. OB contribute to the anabolic process by depositing organic material such as collagen, alkaline phosphatase (ALP), osteopontin (OPN) and osteocalcin (OCN) in ECM, and leads to the formation of hydroxyapatite; ultimately giving bone its mechanical properties (such as strength and elasticity) . They also differentiate into OCy [4,5]. Conversely, OC mediate the catabolic process by breaking down organic material within ECM. OCy are widely regarded as the main mechanosensory cell within bone, therefore they orchestrate the balance between the catabolic and anabolic process via communication with OBs and OCs via ligands such as TGF-beta[3]. It is noteworthy that signalling through sex hormones is believed to play an important role in osteoporosis development, where four out of five cases develop in post-menopausal women and one out of five in aging men. Hence, OCys are continuously exposed to dual biochemical and mechanical (bio-mechanical) cues. Using intracellular signalling mechanisms, they sense, integrate and respond to these stimuli to maintain the balance between catabolic and anabolic events. Disturbance of this balance leads to osteoporosis.

Integration of the bio-mechanical cues, and their transduction into cellular responses, within the BRU, are conducted by intracellular activities such as the mechanotransduction process (figure 1). Mechanotransduction involves the sensation of mechanical forces through mechanoreceptors such as integrins[6-9]. Mechanical signals are converted intracellularly into biochemical reactions via pathways

such as the Extracellular Regulated Kinase (ERK)[10,11]. The ERK pathway is involved in the expression of ECM proteins that control bone material properties and mineral density (BMD), such as OCN and OPN. Recently, dual bio-mechanical stimulation with intermittent parathyroid hormone (PTH) treatment and mechanical stimulation were shown to increase BMD and bone formation in mice, thus suggesting a promising treatment for osteoporosis[12,13]. Furthermore, it was demonstrated that bone density can be increased before and during the menopause using mechanical loading regimes such as resistance training, thus limiting the risk of osteoporosis development. However, precise regimens required to induce a potent therapeutic effect are yet to be determined. This is due to incomplete understanding of the intricate interactions between the different components across scales, and the dynamic stimulations exerted on cells within the BRU [14-17]. Therefore, there is a need to develop methods and tools to advance our understanding of the interactions between the different components, and consequently assist in the development of novel treatment for osteoporosis [5,18,19]. One avenue towards this is to comprehend the interplay between bio-mechanical cues, mediated through mechanotransduction and their influence on cellular responses controlling ECM material properties[20,21].

This study presents a computational approach where a hybrid multiscale model, combining a mechanical model with the agent-based approach (Mech-ABM), was utilised to examine modulation of bio-mechanical signals and their influence on cellular events leading to the expression of ECM proteins (ECMp) that modify bone material properties (such as ALP and BSP). Simultaneously, an analytical mathematical method was used to extract key information from the noise within mechanotransduction, to elucidate the significant impact of the dual alteration on ECMp expression. This study demonstrates that dual modulation of mechanical stimuli and mechanotransduction dynamics, at the level of the ERK pathway, impact modalities of ECMp mRNA expression and that the activation state of integrins may contribute to the shift of the system dynamics, that ultimately contribute to the emergence of osteoporosis[17,20,21]. Furthermore, Mech-ABM and the analysis method further emphasise the

importance of interfering with interactions within Raf-MEK-ERK (Rapidly Accelerated Fibrosarcoma-MAPK/Erk kinase-Extracellular signal-regulated kinase) module to develop candidate pharmaceutical molecules, which add potency when combining bio-mechanical stimulations for future osteoporotic therapies.

Methods

The study examined the impact of dual modulation of bio-mechanical on molecular and cellular responses which impact ECM composition and ultimately its material properties. These are centred around modulation of gene expression and translation of ECMp. This was achieved via utilisation of a multiscale hybrid mechanical-agent based model (Mech-ABM) (Figure 1) as published previously[8]. Briefly, the ABM was used to mimic the dynamic interplay between mechanical stimulation, and intercellular response within a 3D spherical OB embedded within a non-demineralised bone ECM. The ABM simulated mechanotransduction downstream of the integrins mechanoreceptors, which recruited the focal adhesion protein (FAK) and the ERK signalling pathway and led to the synthesis and deposition of extracellular matrix (ECM) proteins (figure 1 a) [8]. The cell was separated to two main compartments, the cytoplasm and the nucleus, which were separated from each other and the ECM by membranes. The agent molecules, each of which is represented as a discrete interacting entity, were assumed to be homogeneously distributed inside their respective compartments, and their movement was described via Brownian motion. These agents (including the cell, see supplementary table-1) were communicating X-machines which rely on state transitions, memory and transition functions to execute processes. Supplementary figure-1 illustrates a representation of all the molecular interactions and types of molecules simulated. The ABM did not include sophisticated organelles such as the Golgi apparatus.

Molecule-molecule interaction, binding events and activation-deactivation state transition (via activation cycles switch (ACS)) are the driving mechanisms of ABM. Furthermore, the Mech-ABM integrated stochastic processes that updated every agent's global and local variable over time; specifically ACS [22]. These were derived from probability functions Ψ(t)[22-24].

The mechanical model mimicked, at the tissue level, the tissue biomechanics and associated mechanical perturbation, as detailed previously[8]. Briefly, a mechanical shear stress was applied at an infinite 3D composite representing the bone ECM; the mechanical forces were transmitted through the ECM to the ECM-cell interface, where integrins (represented as springs) formed the connection between the ECM and the cell. The mechanical force stretches the integrins, and at a particular mechanical threshold, activates them, hence initiating intercellular mechanotransduction. Accumulated number of protein-agents and mRNA-agents over time (24 h) partitioned by their state variables (e.g. active/inactive and bound/unbound) was the primary output analysed from the Mech-ABM. The external mechanical perturbation was a periodic square wave characterized by the amplitude M and the oscillation period P. Modulation of mechanical cues were examined by varying the M (M = 100 and 10,000 μPa) and P (P = 1000, 5000 and 20,000 s). Within the range of P values investigated, two were much shorter than the total duration of the sampling period, named epoch, and in one occasion, the period was set so that the stimulation applied was constant for the entire simulation. The biochemical perturbation was achieved via modulating intercellular molecular interactions within the ERK pathway associated with protein activation cycle (i.e. feedback loops). Total number of simulations was 1800, with 15 repeats per condition.

Re-scaling the 3D interaction volume of agents in the system and the number of agents, accordingly, has little impact on overall rates of intracellular reactions within an ABM framework, if the system does not become excessively sparse and there is enough statistics as demonstrated by Rhodes et al 2016[25].

Hence, the size of a large system of molecules, such as an osteoblast, can be reduced without losing the complexity of the dynamics.

From the simulated processes, the resulting signals representing the number of molecules in a given molecular state, show a series of spikes (prominent peaks), rapid abrupt variations in the signal, which appear to be unsynchronised with the external mechanical perturbations. Nor do the times in between these spikes present a narrow distribution, typical signature of periodicity, neither are they synchronized by repeating the stimulation periodically multiple times with identical mechanical loads. Nevertheless, such spikes are characterized by amplitudes of several molecules of magnitude which imply a form of synchronization despite the non-periodicity. In the long run and for an infinite number of molecules, these fluctuations may asymptotically disappear; yet, there exists a scale where they cannot be neglected and cooperative molecular phenomena have various biological functions[14,16]. However, information regarding the complexity of a non-ergodic system and pattern of activation can be obtained. This was achieved by using an analytical method utilising subordination theory[26,27] as published previously[35]. Briefly, the signal (fluctuating activation spikes) was transformed, via a filter (equation 1 and 2) due to the inherent stochasticity of the system and therefore the ensuing temporal variations in the output (fluctuating signals):

$$\overline{y_i}(t) = \widehat{A}_{\Delta_T} y_i(t) \xrightarrow{\Delta_T \to \infty} \overline{Y_i}(t), \tag{1}$$

$$\widehat{A}_T = \frac{1}{\Delta_T} \int_t^{t+\Delta_T} (\cdot)\, dt'. \tag{2}$$

where $\hat{A}_{\Delta T}$ is the moving average operator over a time period $[t, t + \Delta T]$, and $\underline{y_i}(t)$is the averaged signal with reduced level of noise.

A numerical method utilising subordination theory was used to disentangle random processes into their respective parent process and directing process in order to analyse the latter in terms of patterns of recurrence of events[26]. This was achieved by applying a subordination process separating natural time and the physical time (the macroscopic and experimentally observable time). A moving average filter with a Hilbert transformation was applied twice, thus determining signal time series and amplitude as positive definite time series with enhanced prominent peaks and dumped valleys close to the zero axis. The peaks are detected as events $\mathcal{E}$, if the signal minus one standard deviation σ_i of the fluctuations drops after each peak, $p_n(t)$, below the corresponding preceding peak value:

$$\mathcal{E} = [[p_n(t_1),\ \exists\, t_2 \ \mid\ y_i^{III}(t_2) - \sigma_i(t_2) < y_i^{III}(t_1)]] \qquad (3)$$

Therefore, critical events can be detected and provide detail on repetition of large oscillations within the number of molecules that rapidly reach or depart from a given node within the network. The probability density obtained by normalizing the integral distribution to 1 was expressed as a waiting time distribution (WTD). WTDs between peaks or the time extent of peaks are considered. WTDs are built by sampling the occurrence of peaks for an epoch of time much larger than the average time of two consecutive peaks. a Kernel Density Estimator (KDE) defined as:

$$\text{KDE}(t) = \tfrac{1}{w} \int_t^{t+w} K(t-\tau)(\cdot)d\tau \text{ such that } \int_{-\infty}^{\infty} K(t)\,dt = 1 \qquad (4)$$

w is the support of the operator. Due to the stochasticity within the model and the applied mechanical stimulation, the critical events would approximately result in a complex overlapping of convolution of exponentially distributed processes characterized by multimodality.

WTDs are dependent on the selected parameter for analysis, thus it reflects the specific dynamics of Mech-ABM. The integrated nature built-into the Mech-ABM and those of the mechanical excitation result in the critical events being gamma distributed and typified by modalities. This distribution is used to derive signal interim periods (SIP) τ between consequent events with the magnitude of the

fluctuation. The area τ multiplied by the magnitude measures the minimum time cumulated by a particular molecule, at a given activation state, and the length of time it is involved in the same critical event. The total number of molecules within the same critical event sampled in the entire duration of the sampled signal was demonstrated by the non-normalized distribution. Subsequently, WTD, $\psi(\tau)$ is the probability density obtained by normalizing the integral distribution to 1. In this study the WTD of integrins, ECMp mRNAs and ECMps were illustrated as they are considered as primary osteogenic markers in addition to being amongst the primary components that reflect ECM alteration in response to dual modification in bio-mechanical signal [4,28,29].

Simulations and sensitivity analysis

Creating the dual modulation of bio-mechanical cues on the dynamics of mechanotransduction, and gene expression events were investigated by modifying the external mechanical perturbation and intracellular feedback loops of the ERK pathway. With respect to mechanical excitation it was via changes to the magnitude (*M)* and oscillation period (*P)*, while for the feedback loops, it was achieved by modulating agents Activation Cycle (AC) times $T_{\bullet \to \bullet}$ ($\bullet \to \bullet$ represents the initial and final transition states) for: $T_{RAF_{act}+MEK_d \to MEK_{act}}$, $T_{MEK_{act} \to MEK_d}$, $T_{MEK_{act}+ERK_d \to ERK_{act}}$, $T_{MEK_{act}+ERK_d \to MEK_{act}}$, $T_{ERK_{act} \to ERK_d}$, $T_{ERK_{act}+RUNX2_d \to ERK_{act}}$. For repeatability, the model was simulated for 10 independent runs, though with identical initial conditions for each simulation, the distribution was computed and the 10 independent results were used to generate confidence intervals. The top and bottom of confidence intervals around the WTDs are not probability functions. The generic ABM platform FLAME (Flexible Large-scale Agent Modelling Environment) was used to simulate intercellular mechanotransduction and mechanical loading[30-33]. At t_0, Mech-ABM contained 8890 agents and ran with a unit time step corresponding to 1 second for approximately 24 h. The agents' 3D coordinates within the cell and velocity at t_0 were randomly selected from a uniform distribution. The mechanical load applied at the tissue level was a periodic square wave function defined by its magnitude *M* and oscillation period *P*, the minimal magnitude was 100 μPa and

the phase was set to zero *(see supplementary table* 2). The simulations were run at the SHeffield Advanced Research Computer cluster (SHARC) on machines with 2 x Intel Xeon E5-2630 CPUs and 64GB of RAM. Each simulation required 8GB of RAM, 96 hours of execution time and approximately 500GB of hard disk space.

The parameters explored during this study included two values for M, 3 values for P and 5 values for the 6 selected ACS parameters. The exact values of the aforementioned parameters were provided in supplementary table 3. With n = 10 for each simulated condition, the total number of model runs was 1800. The data obtained from these runs were uploaded to Google Drive (https://drive.google.com/open?id=1Q0HFuvmv6NTxpBXfKQerR93I-4_t9LAu).

Results

Modulation of the ERK pathway Activation Cycle Switch (ASC) with constant mechanical stimulation reveals characteristic mRNA activation dynamics.

From the analyses of occurrence of critical events, mRNAs of OCN, OPN and ALP, bound to ribosomes show similar dynamics, therefore, we have used the results of ALP as an example. As illustrated in figures 2 and 3 for ERK's ACS ($T_{MEK_{act}+ERK_{d}\rightarrow ERK_{act}}$) = 1320 s, the WTDs of mRNAs bound to ribosomes are trimodal and the corresponding peaks are at τ_1 = 4 s, τ_2 = 10 s and τ_3 = 18 s, respectively. The shapes of the WTDs remain constant at all the epochs simulated with the exception of the mode at larger recurrence time τ_3 which tends to fluctuate due to stochastic noise. These properties hold true for P equal to 1000 s and 5000 s (see figure 2a and figure 2b), but looking at the system far from the initial condition at time t_0 and more precisely after an age of t = 5000 s of simulated time, and under constant mechanical loads, the WTDs lose their trimodality and become bimodal as shown in figure 3a and figure

3b. Similarly, in figure 3c the WTDs for MEK ACS ($T_{MEK_{act}+ERK_d \rightarrow MEK_{act}}$) = 1320 s and P = 200000 s have three modes at τ_1 = 4 s, τ_2 = 10 s and τ_3 = 18 s. After the system reaches the age of t = 5000 s, the mode at τ_3 disappears while the other two modes remain at equal τ, figure 3d. In all other cases, the WTDs of mRNAs bound to ribosomes are bimodal. **Systems under constant mechanical loads with large activation times of MEK or ERK have dynamics characterized by bursts of translation occurring at SIP smaller than 10 seconds. In contrast, for periodic mechanical loads, there is a larger probability that abrupt variations in mRNA translation are separated by SIP twice as long**.

Free mRNAs have completely different WTDs compared to their bound counterparts. Generally, all the free mRNA WTDs have modes at SIP equal to τ_1 = 5 s, τ_2 = 41 s and τ_3 = 55 s which are the same at all epochs for any of the values of ACS (i.e. ($T_{\bullet \rightarrow \bullet}$) = 8 – 1320 s), P and M considered (figure 4). The SIP range between τ_1 and τ_2 is characterized by multiple peaks changing with the age of the system as illustrated in figure 4a. Except for $T_{MEK_{act}+ERK_d \rightarrow ERK_{act}}$ < 300 s, in the WTDs of free mRNAs there is a stable peak around τ_4 = 100 s and an oscillating tail which slowly decays until the next stable mode at τ_3. Instead, for values of $T_{MEK_{act}+ERK_d \rightarrow ERK_{act}}$ smaller than 300 s, there is no stable peak at τ = 100 s and decaying tail becomes a long fluctuating plateau, see figure 6b. **Consequently, faster activation of ERK induces a more focused transcription of mRNAs, while at larger values of $T_{MEK_{act}+ERK_d \rightarrow ERK_{act}}$, there is a wide set of SIP between τ_1 and τ_2 with high probability that causes nonrhythmic rapid variations of mRNA production.** It is important to emphasise that consistency of behaviours among all types of mRNA, which in the ABM are identically interacting molecules and are dynamically indistinguishable, showing the reliability of the fluctuation analyses and the robustness of the method.

Shifting integrin activation dynamics and their response to mechanical stimulation is dominated by mechanical stimulation frequency (P) and then by ERK ACS.

With respect to mechanical perturbations, for all the analysed epochs and the simulated periods (P), the results supported that mechanical perturbation was a key trigger of events, with integrins as the main mediators. As the mechanical stimuli cease, eventually signal propagation terminates and the number of activated molecules approaches zero. For active integrins, increasing P by a multiple of 40 resulted in reduction of the variability among independent repetitions of the simulations. In the first and second rows of figure 5, the WTDs with P = 5000 s present a tail with a large confidence interval, and at large τ, the shapes largely fluctuate among different epochs. Instead, for P = 200000 s, the waiting times produce clear bimodal distributions with reduced confidence intervals at large τ resulting in no tail and a stable shape during different ages. The reduction of noise on active integrins' SIP is strongly sensitive to the length of the period P, but not on the magnitude of the perturbation, figure 5b. The increase in M allows for increased molecular interactions within mechanotransduction, thus it is expected that the number of events increase and so does the area under the histograms; nonetheless WTDs do not change significantly. The data demonstrate that the sensitivity to P for active integrins' SIP does not depend on the value of $T_{RAF_{act}+MEK_d \rightarrow MEK_{act}}$, $T_{MEK_{act}+ERK_d \rightarrow MEK_{act}}$ and $T_{MEK_{act} \rightarrow MEK_d}$; however, when the ERK cycle is slowed down, corresponding to $T_{MEK_{act}+ERK_d \rightarrow ERK_{act}}$, $T_{ERK_{act} \rightarrow ERK_d}$ and $T_{ERK_{act}+RUNX2_d \rightarrow ERK_{act}}$ larger than the baseline values, the WTDs noisy tails disappear, and the distributions are the same for any value of the perturbation period.

Ageing characteristics are observed at the level of nuclear events

The system presented previously demonstrated an aging characteristic[35] at the level of the ERK pathway. This aging is a feature that is a direct consequence of the initial conditions and corresponds to a slow variation of the WTD as time passes. *Viz*., where initial conditions and perturbations (such as those of P) might impact the emergence and frequency of critical events monitored, and hence WTDs. Among all

molecules analysed, transcribed factors are characterized by ageing with an evident and clear progression. From the integral distributions in figure 6, we observe that, with the increase of age, there is a reduction of the number of abrupt fluctuations. A similar ageing effect appears in all the mRNAs bound to ribosomes. However, in many cases analysed, the corresponding WTD does not show sufficient discrepancies between different epochs; signifying that dispersion times decrease with the same amount as time passes, and the ageing effect is reduced to a slowing of the system dynamics. As a direct consequence of the fixed number of total ribosomes simulated in the cytoplasm, ribosomes in their free state also present an ageing effect, but their dispersion times increase with the age of the system. For free mRNA, the variations with the age t of the dispersion times change at different rates depending on the SIP value τ *so* their WTD does not preserve the shape, but changes from a trimodal distribution to a bimodal distribution as time passes, figure 4.

Discussion

The study shows that it is feasible to extract informative detail from the naturally chaotic mechanotransduction-mediated gene expression events in OBs. This information can provide additional prospective regarding the shift in the system's dynamics due to modulation of bio-mechanical cues. It further supports that modulation of the molecular interactions of Raf-MEK-ERK module can provide innovative targets for the development of new drugs for osteoporosis. These outcomes were feasible via utilisation of the hybrid-multiscale Mech-ABM and an analytical method that utilised subordination theory.

Osteoporosis develops due to reduction in the efficiency of the anabolic mechanisms of maintaining ideal bone material properties and strength. This is directly related to OBs response to bio-mechanical stimulus, where OBs deposit ECMps and differentiate to OCy. Mechanotransduction plays an important

role in mediating these events. Hence, inducing OBs towards osteogenic response at the level of mRNA transcription and translation is important. How dual bio-mechanical stimuli achieve this is poorly understood. Nonetheless, we previously demonstrated that fluctuations in the system (OB's mechanotransduction) is beyond mere system randomness[34], and that with dual alteration of mechanical load and ERK's feedback loops (i.e. ACSs), the WTDs can reflect molecular signatures of the system with respect to cytoplasmic events. In this study, increasing ACS caused a shift in modalities of free mRNA, making gene transcription events more chaotic and frequent, as illustrated with reduced levels of ALP mRNA, increased WTDs modalities, and an expanded tail. This demonstrates that modulation of ERK activity can shift cellular response and enhance the expression of ECMp. This observation agrees with the proposals Yang et al had made recently that the ERK cascade is important in orchestrating mechanotransduction and is vital for maintenance of ECM within bone[11]. Additionally, this impact on osteogenic gene expression is in line with in vitro studies showing that inhibition of ERK activation antagonises RUNX2 nuclear activity and thus reduces the expression of ALP and OCN, ultimately reducing ECM mineralisation[35]. Tomida et al demonstrated similar behaviour in inflammatory systems, whereby they showed that asynchronous oscillatory activation of the MAPK protein and ERK relative, p38, generated a burst of activity of inflammatory genes[36]. Furthermore, it was demonstrated previously that modulated stochastic and pulsatile activity of ERK could modify homeostatic gene expression events and drive cell proliferation when nudged by external signals[37-39]. Consequently, this further suggests that mechanical signals can impose a nudge-effect on ERK signalling towards anabolic activity by stabilising the WTD.

The results presented here illustrated that the ensuing gene expression events of bio-mechanical signals, in contrast to cytoplasmic mechanotransduction events[8,34], are noisier. These chaotic events were particularly evident at the level of transcribed ECMp mRNAs (e.g. free ALP mRNA, figure 4) and translated mRNA (figures 2 and 3). The latter was measured by the number of activated mRNA- bound

to ribosomes. The eruption of activity at the gene expression level, following conservative activation activity in the cytoplasm by the ERK module, is in line with physiological observations[40,41]. Furthermore, our observation that the period of mechanical stimulation causes a shift in the dynamics of the system, by shifting WTDs modality from one value to another, is equivalent to in vitro studies demonstrating that short bursts of mechanical stimulations can elicit potent cellular response[42,43].

This is probable considering that the most significant impact on mRNA magnitude and WTD modalities was observed with dual manipulation of mechanical load and ERK's ACS. Increasing P and ERK ACS has resulted in a more pronounced shift in WTDs' modalities, whereby multi-modalities shift to either tri- or bi modalities. This suggests that dual change of bio-mechanical stimulation drives the system, and in particular ECMp mRNA levels, from somewhat chaotic and frequent, to stable and specifically expressed at particular SIPs. This suggests that mechanical stimulation in the form of P acts as coincidence detector and filter, selecting ERK induced SIPs that will propagate optimum mRNA transcription and translation events for osteogenic markers such as ECMps; thus substantially augmenting ECMp deposition. These decisions ultimately influence bone density and BMD. This is in line with the work of Albeck et al who demonstrated that within genetically identical sister cells, bursts of asynchronous ERK activities determine if cells entered S-phase and thus the dynamics of cell proliferative response to epidermal growth factor (EGF) stimulation[37].

As it was demonstrated previously that biased PTH receptor (PTHR) agonists recruit the Raf-MEK-ERK module and enhance its signalling impact[44-46], we provide another avenue to explore new therapies where protein interactions within the module can be altered using small peptides. The candidate molecules can be scaffold proteins such as KSR or beta-arrestins. The latter has links with PTH receptor (PTHR) and was shown to be the mediator of the biased agonism[44,45]. This is a credible suggestion since

the use of small molecules aimed at intracellular molecular targets have been explored recently and showed a degree of promise[47-49].

Limitations:

We acknowledge that our Mech-ABM uses assumptions and constraints that will put some restrictions on what to infer from the data. For example, mechanical stimulation does not change the spherical shape of the cell over the course of the simulation and this might impose a restriction on the propagation of the mechanotransduction. We also recognise that to draw a full conclusion on ECM health over time, the model should be simulated for a longer period, at least a few days, to see the long-term effect of dual bio-mechanical stimulation on cell behaviour. However, this is computationally costly, and will require adjustment of the model to overcome this issue. Furthermore, we appreciate the role sex hormones and their involvement in osteoporosis progression; however, these are outside of the scope of the Mech-ABM as its cell signalling network does not include the hormonal component. Yet incorporating these into the model in the future is uncomplicated and is achievable. Though we realise there are limitations, nonetheless, thus far the model has replicated physiological phenomena and the emergent behaviour of bio-mechanical stimulation consistent with physiological observations both in vitro and in vivo. These give us great confidence in the interpretations made using it.

Conclusions

We observed large fluctuations enclosing information hidden in the noise which is beyond the dynamic variations of molecular baselines. These were observed as alterations in WTD of free and activated mRNA for osteogenic markers (e.g. ALP and BSP). Therefore, WTDs of each molecule are a signature of the system's dynamics. In contrast with more traditional approaches, where noise has been adopted as

a measure to quantify the error around the expected values of time dependent signals. In our study, the abrupt fluctuations departing from the trend have been explored and analysed, thus hidden information characteristic to mRNA molecules and of the process' dynamics were extracted. These forecast protein-protein interactions at the level of RAF -MEK-ERK module to play a key role in dual bio-mechanical signalling. Thus, modulation of scaffold proteins could be an innovative approach to modify mechanotransduction and ultimately develop innovative therapies for osteoporosis.

Competing interests

The authors declare that they have no competing interests.

Acknowledgements

We would like to thank Mis Yasmin Beladaci for her effort in generating preliminary data which assisted in parameter evaluation. This study was funded by the Engineering and Physical Sciences Research Council (EPSRC), Frontier Engineering Multiscale modelling of the skeleton: EP/K03877X/1

Data Availability Statement

Our code, data and appropriate materials are available under the Creative Commons Attribution License. These are available on Google Drive with the following hyperlinks:

(https://drive.google.com/open?id=1Q0HFuvmv6NTxpBXfKQerR93I-4_t9LAu).

Authors' contributions

GA and AS wrote the manuscript, GA designed and performed the model analysis, and executed the simulations; AS, TMS and DL designed the Mech-ABM; AS lead the *in silico* experimentation design and sensitivity analysis parameter selection, EDA and AS contributed equally to: in silico experimentation refinement, analysis framework for the model, and data interpretation. DL, TMS, EDA and AS edited the manuscript.

Author details

[1] Department of Oncology and Metabolism, University of Sheffield, Sheffield, UK,

[2] Insigneo Institute of In Silico Medicine, University of Sheffield, Sheffield, UK,

[3] Department of Mechanical Engineering, University of Sheffield, Sheffield, UK

Figures

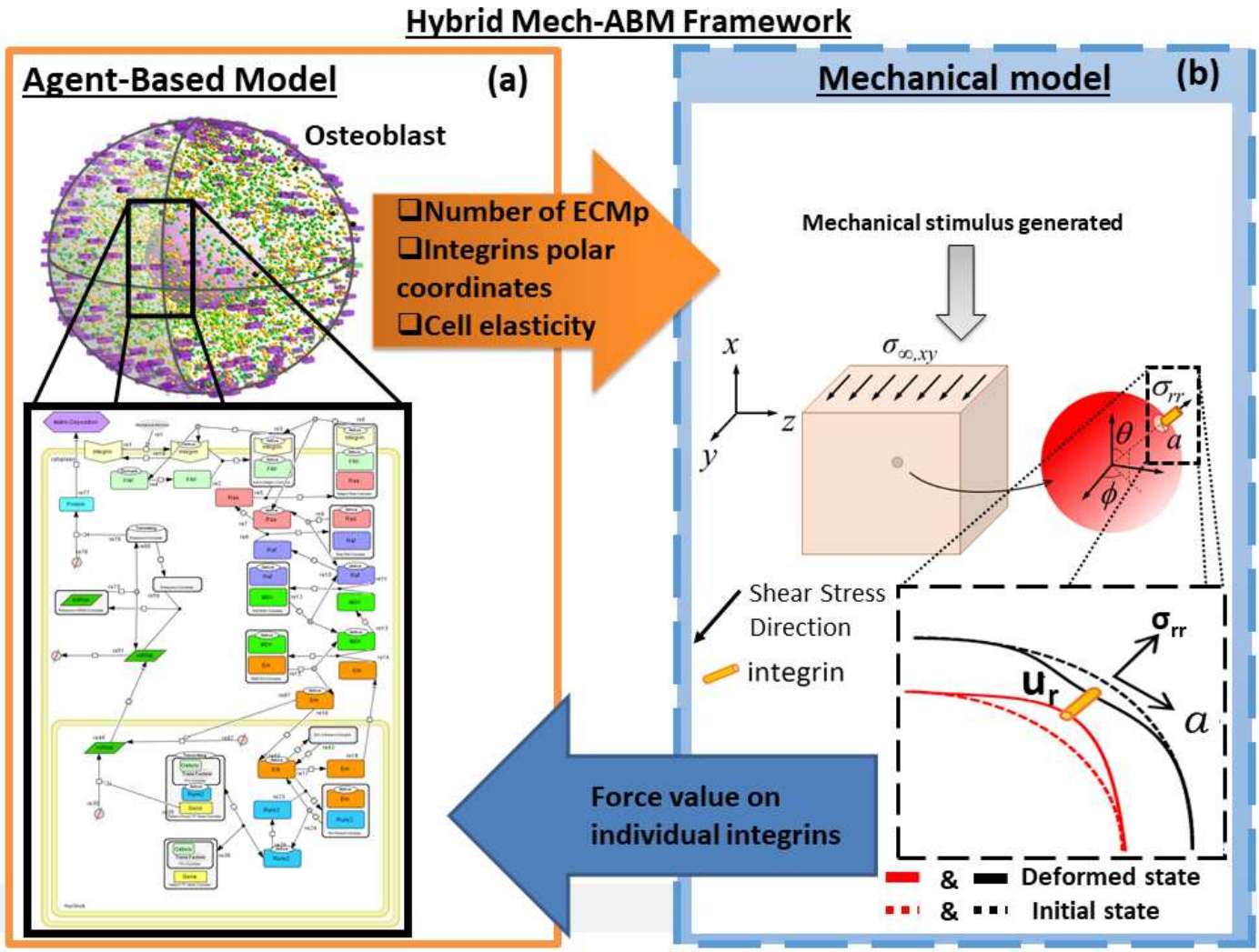
Hybrid Mech-ABM Framework
Agent-Based Model
(a)
Osteoblast
❑Number of ECMp
❑Integrins polar coordinates
❑Cell elasticity
Mechanical model
(b)
Mechanical stimulus generated
Shear Stress Direction
integrin
Force value on individual integrins
Deformed state
Initial state

Figure 1 Simulating dual biochemical and mechanical excitations using a hybrid multi-scale model.

The model simulates mechanotransduction within a single osteoblast, and links the outcome to a mechanical model that handles the biomechanics at the tissue scale. (a) The mechanotransduction cascade was modelled from the integrin mechanoreceptors and involved the recruitment of the Raf-MEK-ERK signalling module in the cytoplasm; this resulted in the activation of nuclear events and the mRNA expression of osteogenic markers such as bone sialoprotein (BSP) and alkaline phosphatase (ALP). mRNA is translated to their corresponding proteins when they interact with activated ribosomes. The mechanotransduction cascade was represented using the System Biology Graphical Notations (SBGN), a detailed diagram was provided in supplementary figure 1. (b) A schematic representation of the mechanical model. A mechanical force is generated using a mathematical algorithm that propagates through the tissue composite as shear stress. The mechanical force is transmitted to integrins causing it to stretch; the calculated force on the integrin determines its activation. The force value is calculated and passed to the ABM to determine if integrins become fully activated and thus the propagation of mechanotransduction. The large arrows indicate the information passed between the two models. The two models are in contact every iteration, which is equivalent to 1 s.

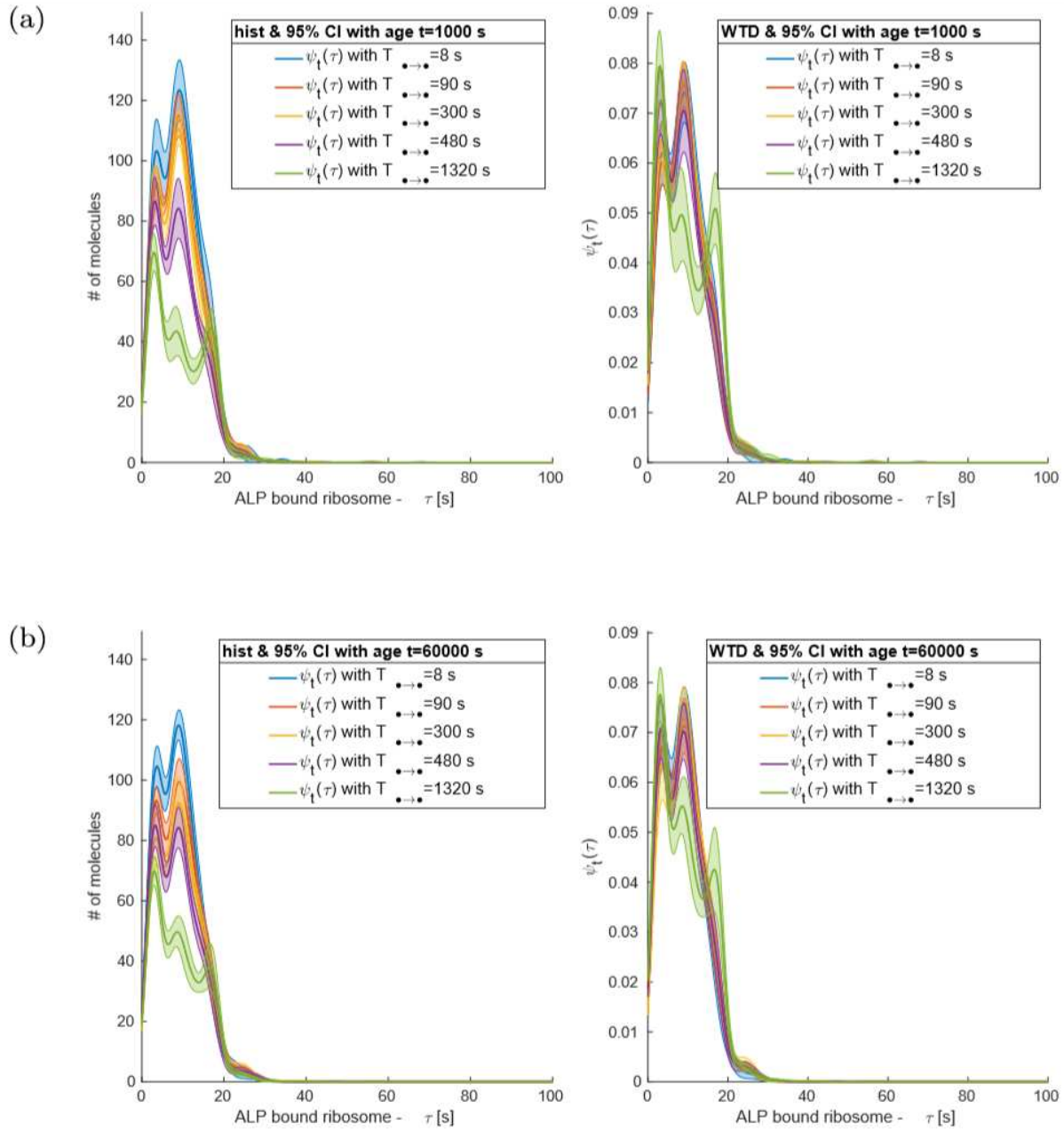
(a)
hist & 95% CI with age t=1000 s
WTD & 95% CI with age t=1000 s
(b)
hist & 95% CI with age t=60000 s
WTD & 95% CI with age t=60000 s
# of molecules
ALP bound ribosome - τ [s]

Figure 2 Ageing of ALP mRNA.

For $T_{MEK_{act}+ERK_{d}\rightarrow ERK_{act}}$ = 1320 *s*, the WTDs of the ALP mRNA have trimodal distributions with peaks at 4 *s*, 10 *s* and 18 *s*. The three modes are persistent at any age of the system. For $T_{MEK_{act}+ERK_{d}\rightarrow ERK_{act}} \leq 480$ *s*, the WTDs' slope at $\tau > 10$ *s* remains negative and the shape of the WTDs is bimodal. **(a)** and **(b)** $M = 10000$ μPa and $P = 1000$ *s*, while $T_{ERK_{act}\rightarrow ERK_{d}}$ changes; **(b)** aged condition of the case on the above line.

(a)

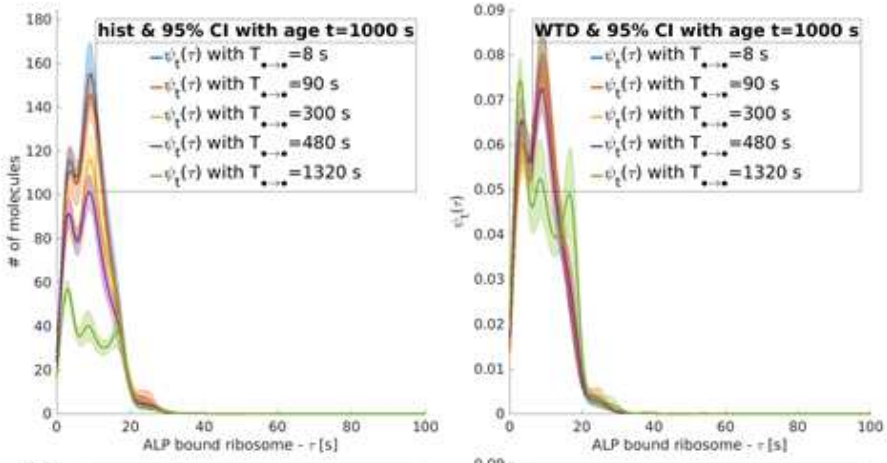
hist & 95% CI with age t=1000 s
WTD & 95% CI with age t=1000 s
# of molecules
ALP bound ribosome - τ [s]

(b)

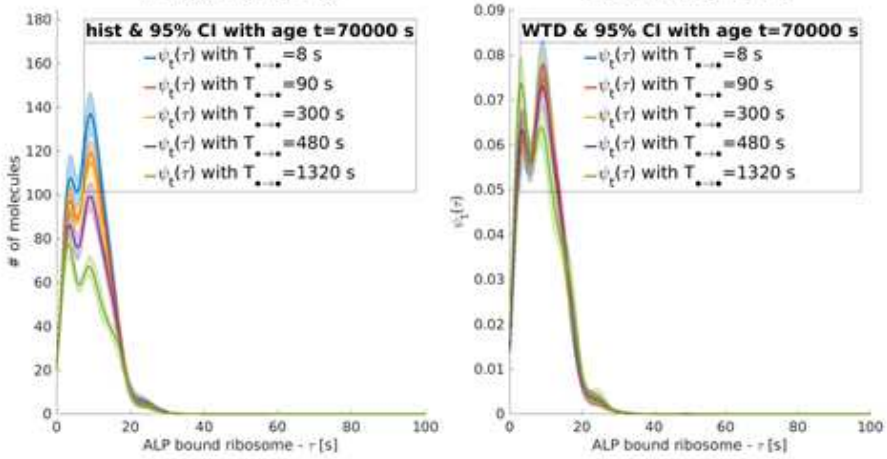
hist & 95% CI with age t=70000 s
WTD & 95% CI with age t=70000 s
# of molecules
ALP bound ribosome - τ [s]

(c)

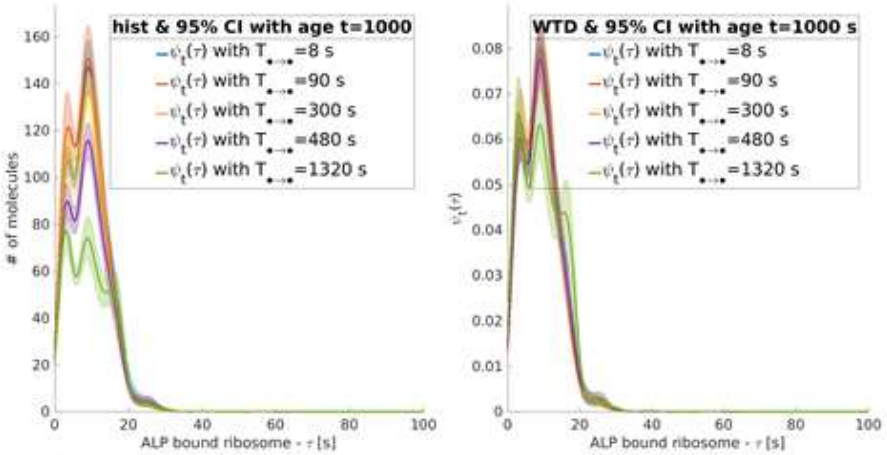
hist & 95% CI with age t=1000
WTD & 95% CI with age t=1000 s
# of molecules
ALP bound ribosome - τ [s]

(d)

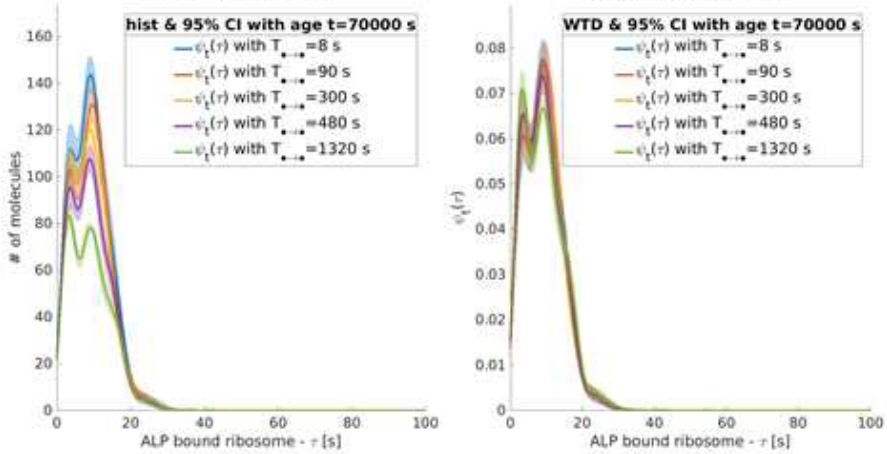
hist & 95% CI with age t=70000 s
WTD & 95% CI with age t=70000 s
# of molecules
ALP bound ribosome - τ [s]

Figure 3 Ageing of ALP mRNA.

For $T_{MEK_{act}+ERK_d \rightarrow MEK_{act}} = T_{MEK_{act}+ERK_d \rightarrow ERK_{act}} = 1320\ s$, the WTDs of the ALP mRNA at $t = 0\ s$ have trimodal distributions with peaks at 4 *s*, 10 *s* and 18 *s*. After the system reaches age $t = 5000\ s$, the WTDs' slope at $\tau > 10\ s$ remains negative. In the other cases, the peak at $\tau = 18\ s$ is not present. **(a)**-**(d)** $M = 10000\ \mu Pa$ and $P = 200000$; **(a)** $T_{MEK_{act}+ERK_d \rightarrow ERK_{act}}$ changes; **(b)** aged condition of the case on the above line; **(c)** $T_{MEK_{act}+ERK_d \rightarrow MEK_{act}}$ changes; **(d)** aged condition of the case on the above line.

(a)

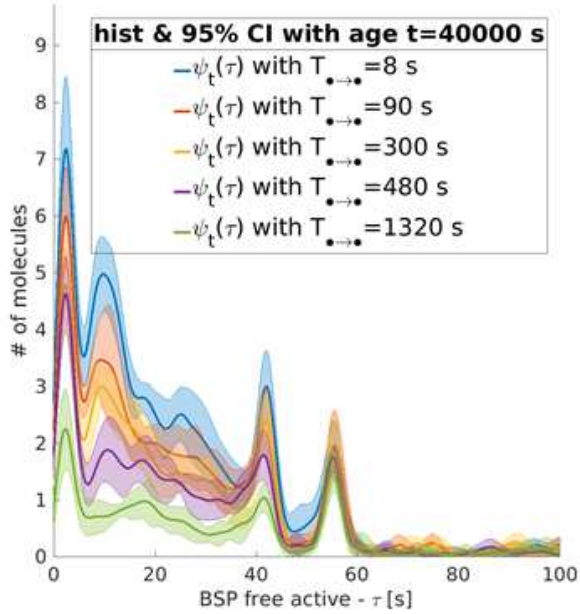
hist & 95% CI with age t=40000 s
$\psi_t(\tau)$ with $T_{\bullet\to\bullet}$=8 s
$\psi_t(\tau)$ with $T_{\bullet\to\bullet}$=90 s
$\psi_t(\tau)$ with $T_{\bullet\to\bullet}$=300 s
$\psi_t(\tau)$ with $T_{\bullet\to\bullet}$=480 s
$\psi_t(\tau)$ with $T_{\bullet\to\bullet}$=1320 s
# of molecules
BSP free active - τ [s]

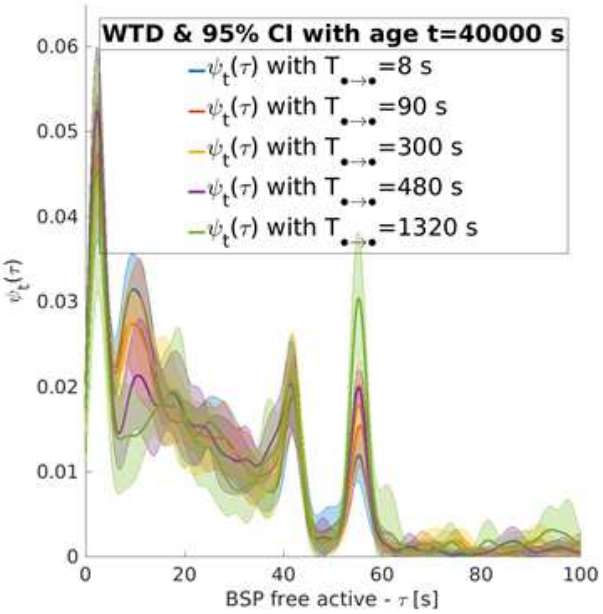
WTD & 95% CI with age t=40000 s
$\psi_t(\tau)$ with $T_{\bullet\to\bullet}$=8 s
$\psi_t(\tau)$ with $T_{\bullet\to\bullet}$=90 s
$\psi_t(\tau)$ with $T_{\bullet\to\bullet}$=300 s
$\psi_t(\tau)$ with $T_{\bullet\to\bullet}$=480 s
$\psi_t(\tau)$ with $T_{\bullet\to\bullet}$=1320 s
$\psi_t(\tau)$
BSP free active - τ [s]

(b)

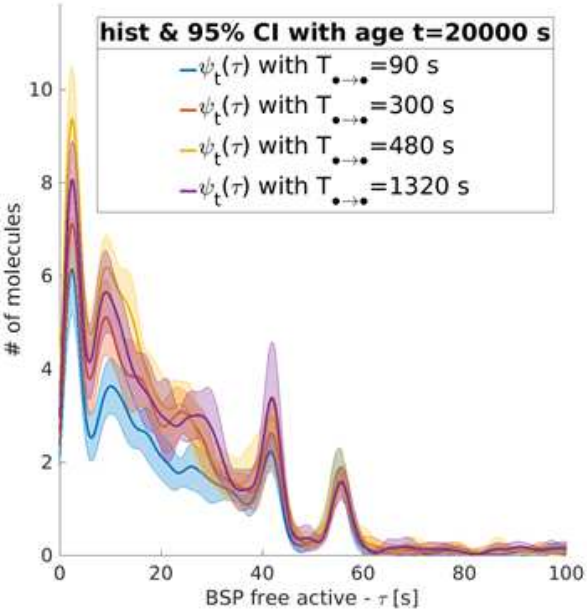
hist & 95% CI with age t=20000 s
$\psi_t(\tau)$ with $T_{\bullet\to\bullet}$=90 s
$\psi_t(\tau)$ with $T_{\bullet\to\bullet}$=300 s
$\psi_t(\tau)$ with $T_{\bullet\to\bullet}$=480 s
$\psi_t(\tau)$ with $T_{\bullet\to\bullet}$=1320 s
# of molecules
BSP free active - τ [s]

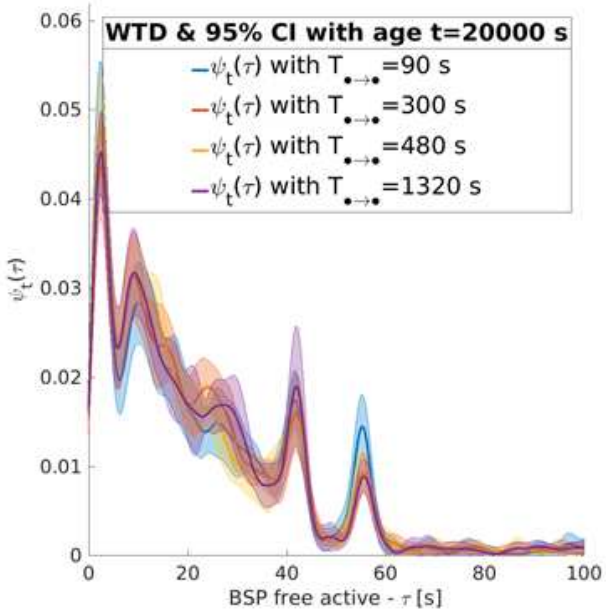
WTD & 95% CI with age t=20000 s
$\psi_t(\tau)$ with $T_{\bullet\to\bullet}$=90 s
$\psi_t(\tau)$ with $T_{\bullet\to\bullet}$=300 s
$\psi_t(\tau)$ with $T_{\bullet\to\bullet}$=480 s
$\psi_t(\tau)$ with $T_{\bullet\to\bullet}$=1320 s
$\psi_t(\tau)$
BSP free active - τ [s]

Figure 4 BSP mRNA.

The BSP mRNA WTDs have 4 modes. The shapes of the distributions are similar to all the unbounded mRNA in the cytoplasm. The modes are at τ equal to 5 *s*, 10 *s*, 41 *s* and 55 *s*. In the region between the modes at 10 *s* and 41 *s*, the distributions are noisy and their average slope depend on $T_{\bullet \to \bullet}$. **(a)** P = 1000 *s*, M = 10000 μPa and $T_{MEK_{act} \to MEK_d}$ change; **(b)** P = 200000 *s*, M = 10000 μPa and $T_{MEK_{act}+ERK_d \to ERK_{act}}$ change.

(a)

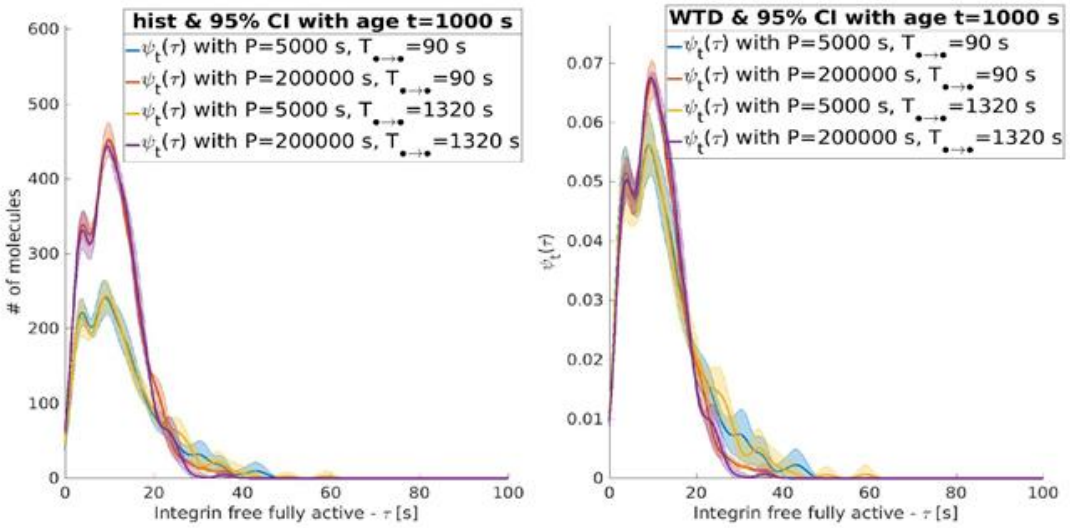
hist & 95% CI with age t=1000 s
$\psi_t(\tau)$ with P=5000 s, $T_{\bullet\to\bullet}$=90 s
$\psi_t(\tau)$ with P=200000 s, $T_{\bullet\to\bullet}$=90 s
$\psi_t(\tau)$ with P=5000 s, $T_{\bullet\to\bullet}$=1320 s
$\psi_t(\tau)$ with P=200000 s, $T_{\bullet\to\bullet}$=1320 s
# of molecules
Integrin free fully active - τ [s]
WTD & 95% CI with age t=1000 s
$\psi_t(\tau)$ with P=5000 s, $T_{\bullet\to\bullet}$=90 s
$\psi_t(\tau)$ with P=200000 s, $T_{\bullet\to\bullet}$=90 s
$\psi_t(\tau)$ with P=5000 s, $T_{\bullet\to\bullet}$=1320 s
$\psi_t(\tau)$ with P=200000 s, $T_{\bullet\to\bullet}$=1320 s
$\psi_t(\tau)$
Integrin free fully active - τ [s]

(b)

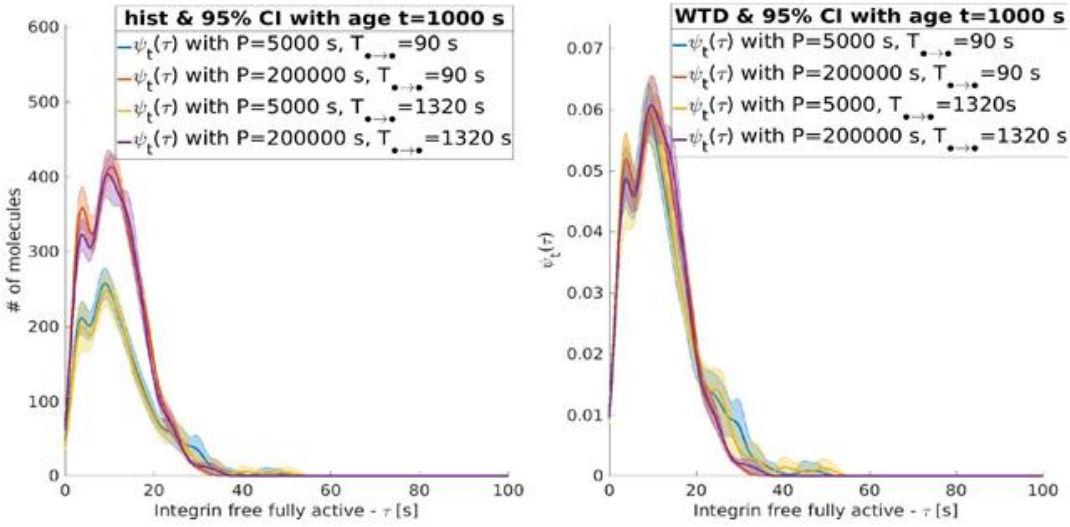
hist & 95% CI with age t=1000 s
$\psi_t(\tau)$ with P=5000 s, $T_{\bullet\to\bullet}$=90 s
$\psi_t(\tau)$ with P=200000 s, $T_{\bullet\to\bullet}$=90 s
$\psi_t(\tau)$ with P=5000 s, $T_{\bullet\to\bullet}$=1320 s
$\psi_t(\tau)$ with P=200000 s, $T_{\bullet\to\bullet}$=1320 s
# of molecules
Integrin free fully active - τ [s]
WTD & 95% CI with age t=1000 s
$\psi_t(\tau)$ with P=5000 s, $T_{\bullet\to\bullet}$=90 s
$\psi_t(\tau)$ with P=200000 s, $T_{\bullet\to\bullet}$=90 s
$\psi_t(\tau)$ with P=5000, $T_{\bullet\to\bullet}$=1320s
$\psi_t(\tau)$ with P=200000 s, $T_{\bullet\to\bullet}$=1320 s
$\psi_t(\tau)$
Integrin free fully active - τ [s]

(c)

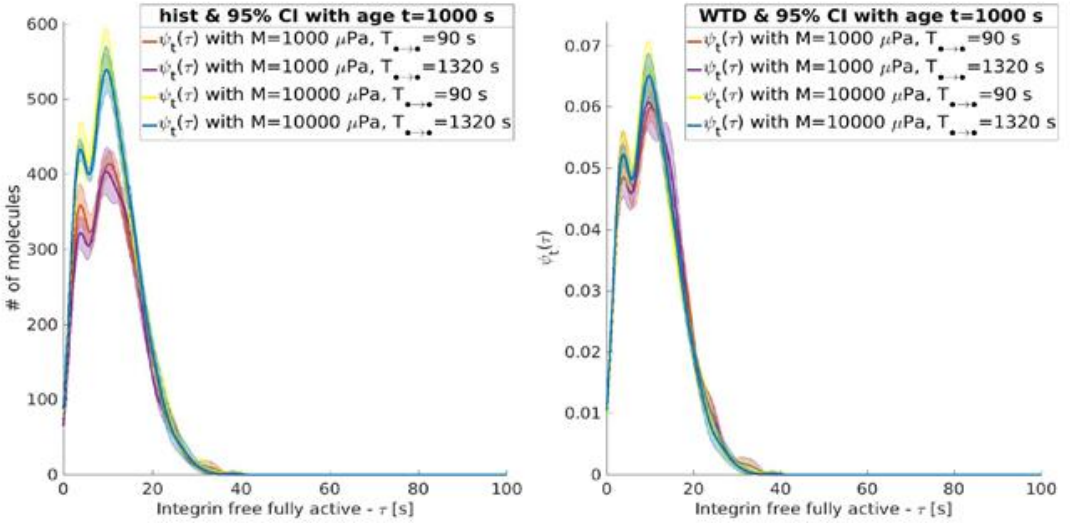
hist & 95% CI with age t=1000 s
$\psi_t(\tau)$ with M=1000 μPa, $T_{\bullet\to\bullet}$=90 s
$\psi_t(\tau)$ with M=1000 μPa, $T_{\bullet\to\bullet}$=1320 s
$\psi_t(\tau)$ with M=10000 μPa, $T_{\bullet\to\bullet}$=90 s
$\psi_t(\tau)$ with M=10000 μPa, $T_{\bullet\to\bullet}$=1320 s
# of molecules
Integrin free fully active - τ [s]
WTD & 95% CI with age t=1000 s
$\psi_t(\tau)$ with M=1000 μPa, $T_{\bullet\to\bullet}$=90 s
$\psi_t(\tau)$ with M=1000 μPa, $T_{\bullet\to\bullet}$=1320 s
$\psi_t(\tau)$ with M=10000 μPa, $T_{\bullet\to\bullet}$=90 s
$\psi_t(\tau)$ with M=10000 μPa, $T_{\bullet\to\bullet}$=1320 s
$\psi_t(\tau)$
Integrin free fully active - τ [s]

Figure 5 Active integrins.

The distribution of recurrence of events for active integrins is bimodal in $T \sim [[3, 12]]$ s. The modes are independent from the periods and the magnitude of the mechanical load. The tail of the distributions at large T are sensitive to the perturbation period P. For P = 5000 s, the distributions show a noisy large tail. For P = 200000 s, the distributions decay rapidly at zero around $\tau \sim 25$ s. At large T, the distribution does not depend on the magnitude M. (a) M = 1000 P a while P and $T_{MEK_{act}+ERK_d \rightarrow MEK_{act}}$ change; (b) M = 1000 P a while P and $T_{MEK_{act} \rightarrow MEK_d}$ change; (c) P = 200000 s while M and $T_{MEK_{act} \rightarrow MEK_d}$ change.

Spectrogram
BSP bound full capacity ribosome
# of molecules
t [s]
τ [s]
$\psi_t(\tau)$
0.0816
0.0612
0.0408
0.0204
0
×10^4

Figure 6 BSP mRNA bound to ribosome.

Spectrogram of the critical events for BSP mRNA during translation. On the x axis, the age t of the non-normalized histogram also corresponding to the beginning of an epoch; on the y axis, the SIP τ; on the z axis, the number of events registered during each epoch of length 10000 s. The vertical black lines crossing the surface show the 95% CI. The colour defines the value of the WTD ψ at SIP τ and age *t*. The WTD is bimodal and the shape is constant at all t. Nonetheless, the total number of critical events decreases with the age.

Supplementary material

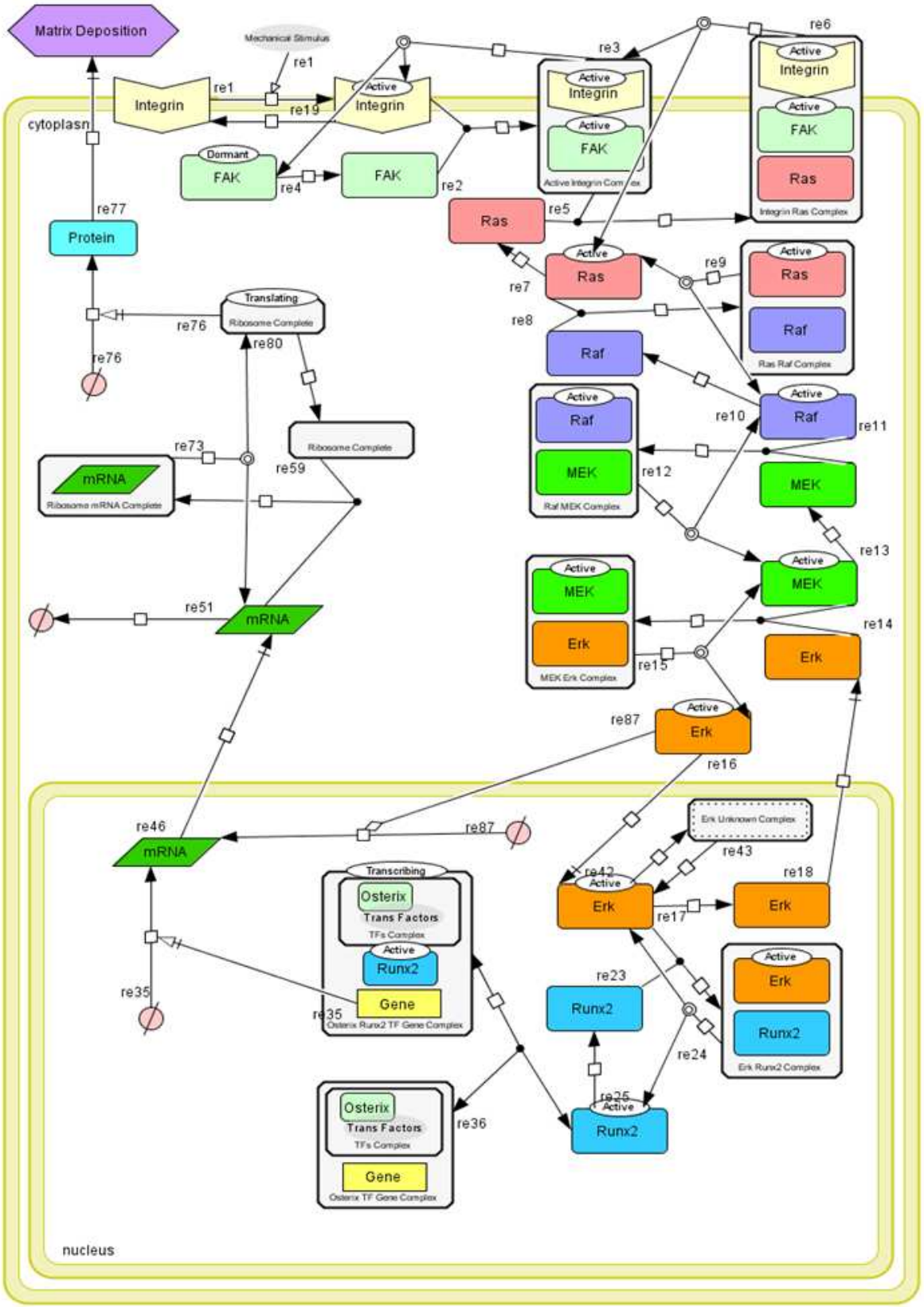

Supplementary figure 1

A system biology graphical notation graph illustrating the mechanotransduction cascade. The molecular interactions between the molecules involved in the pathway were represented and their state transitions were shown.

Molecule	#
Osteoblast cell	1
I_d	500
$I_{f\ act}$	0
$I_{f\ act} + FAK_{act}$	0
I_{act}	0
FAK_{act}	1000
$I_{f\ act} + FAK_{act}$	1
$I_{f\ act} + FAK_{act} + RAS_d$	1
FAK_d	1
RAS_d	1000
$I_{f\ act} + FAK_{act} + RAS_d$	0
RAS_{act}	0
$RAS_{act} + RAF_d$	0
RAF_d	32
$RAS_{act} + RAF_d$	0
RAF_{act}	0
$RAF_{act} + MEK_d$	0
MEK_d	3400
$RAF_{act} + MEK_d$	0
MEK_{act}	0
$MEK_{act} + ERK_d$	0
ERK_d	2300
$MEK_{act} + ERK_d$	0
ERK_{act}	0
$ERK_{act} + RUNX2_d$	0
$ERK_{act} + OTHER$	0
$RUNX2_d$	24
$ERK_{act} + RUNX2_d$	0
$RUNX2_{act}$	0
$RUNX2_{act} + DNA$	0
OSX_{mon}	8
$RUNX2_{act} + OSX_{mon}$	0
$OSX_{mon} + DNA$	5
$RUNX2_{act} + OSX_{mon} + DNA$	0
$RUNX2_{act} + OSX_{mon} + DNA + AP1$	0
OSX_{mul}	5
$RUNX2_{act} + OSX_{mul}$	0
$OSX_{mul} + DNA$	6
$RUNX2_{act} + OSX_{mul} + DNA$	0
$AP1$	0
$RUNX2_{act} + OSX_{\mathbf{mon}} + DNA + AP1$	0
OPN_{RNA}	0
$Rib_{av} + OPN_{RNA}$	0
$Rib_{n\ av} + OPN_{RNA}$	0
OCN_{RNA}	0
$Rib_{av} + OCN_{RNA}$	0
$Rib_{n\ av} + OCN_{RNA}$	0
ALP_{RNA}	0
$Rib_{av} + ALP_{RNA}$	0
$Rib_{n\ av} + ALP_{RNA}$	0
BSP_{RNA}	0
$Rib_{av} + BSP_{RNA}$	0
$Rib_{n\ av} + BSP_{RNA}$	0
$Rib_{n\ comp}$	299
$Rib_{n\ comp} + RNA$	0
Rib_c	301
$Rib_c + RNA$	0
$MAT + Vesc$	0

Supplementary table 1: Number of molecules at t_0

Parameter	Symbol	Value	Unit of measure
Mechanical min. magnitude	m	100	μPa
Mechanical phase	ϕ	0	rad
Integrin activation delay	$T_{\mathrm{I_d}\rightarrow\mathrm{I_{f\ act}}}$	0	s
$\mathrm{I_d}$ dissoc. time from $\mathrm{I}+\mathrm{FAK}$ comp.	$T_{\mathrm{I_{f\ act}}+\mathrm{FAK_{act}}\rightarrow\mathrm{I_d}}$	$U[0,80]$	s
$\mathrm{FAK_{act}}$ activation delay	$T_{\mathrm{FAK_d}\rightarrow\mathrm{FAK_{act}}}$	5	s
$\mathrm{FAK_d}$ dissoc. time from $\mathrm{I}+\mathrm{FAK}$ comp.	$T_{\mathrm{I_{f\ act}}+\mathrm{FAK_{act}}\rightarrow\mathrm{FAK_d}}$	30	s
$\mathrm{I_{act}}+\mathrm{FAK}$ dissoc. time	$T_{\mathrm{I_{f\ act}}+\mathrm{FAK_{act}}+\mathrm{RAS_d}\rightarrow\mathrm{I_{f\ act}}+\mathrm{FAK_{act}}}$	7	s
$\mathrm{RAS_{act}}$ dissoc. time from $\mathrm{I}+\mathrm{FAK}+\mathrm{RAS}$ comp.	$T_{\mathrm{I_{f\ act}}+\mathrm{FAK_{act}}+\mathrm{RAS_d}\rightarrow\mathrm{RAS_{act}}}$	7	s
$\mathrm{RAS_{act}}$ dissoc. form $\mathrm{RAS}+\mathrm{RAF}$ comp.	$T_{\mathrm{RAS_{act}}+\mathrm{RAF_d}\rightarrow\mathrm{RAS_{act}}}$	14	s
$\mathrm{RAS_{act}}$ relaxation time	$T_{\mathrm{RAS_{act}}\rightarrow\mathrm{RAS_d}}$	60	s
$\mathrm{RAF_{act}}$ dissoc. time	$T_{\mathrm{RAS_{act}}+\mathrm{RAF_d}\rightarrow\mathrm{RAF_{act}}}$	14	s
$\mathrm{RAF_{act}}$ dissoc. time from $\mathrm{RAF}+\mathrm{MEK}$	$T_{\mathrm{RAF_{act}}+\mathrm{MEK_d}\rightarrow\mathrm{RAF_{act}}}$	10	s
Relaxation of $\mathrm{RAF_{act}}$	$T_{\mathrm{RAF_{act}}\rightarrow\mathrm{RAF_d}}$	60	s
$\mathrm{MEK_{act}}$ dissoc. time from $\mathrm{RAF}+\mathrm{MEK}$ comp.	$T_{\mathrm{RAF_{act}}+\mathrm{MEK_d}\rightarrow\mathrm{MEK_{act}}}$	10	s
$\mathrm{MEK_{act}}$ dissoc. time from $\mathrm{MEK}+\mathrm{ERK}$ comp.	$T_{\mathrm{MEK_{act}}+\mathrm{ERK_d}\rightarrow\mathrm{MEK_{act}}}$	8	s
MEK relaxation time	$T_{\mathrm{MEK_{act}}\rightarrow\mathrm{MEK_d}}$	88	s
ERK activation time	$T_{\mathrm{MEK_{act}}+\mathrm{ERK_d}\rightarrow\mathrm{ERK_{act}}}$	8	s
ERK relaxation time	$T_{\mathrm{ERK_{act}}\rightarrow\mathrm{ERK_d}}$	50	s
$\mathrm{ERK_d}$ dissoc. time from $\mathrm{RUNX2}+\mathrm{ERK}$ comp.	$T_{\mathrm{ERK_{act}}+\mathrm{RUNX2_d}\rightarrow\mathrm{ERK_{act}}}$	10	s
$\mathrm{ERK_{act}}$ dissoc. time from $\mathrm{ERK_{act}}+\mathrm{OTHER}$ comp.	$T_{\mathrm{ERK_{act}}+\mathrm{OTHER}\rightarrow\mathrm{ERK_{act}}}$	6	s
$\mathrm{RUNX2_{act}}$ dissoc. time from $\mathrm{ERK_{act}}+\mathrm{RUNX2_d}$ comp.	$T_{\mathrm{ERK_{act}}+\mathrm{RUNX2_d}\rightarrow\mathrm{RUNX2_{act}}}$	10	s
$\mathrm{RUNX2_{act}}$ dissoc. time from $\mathrm{RUNX2_{act}}+\mathrm{DNA}$ comp.	$T_{\mathrm{RUNX2_{act}}+\mathrm{DNA}\rightarrow\mathrm{RUNX2_{act}}}$	10	s
RUNX2 relaxation time	$T_{\mathrm{RUNX2_{act}}\rightarrow\mathrm{RUNX2_d}}$	60	s
$\mathrm{OSX_{mon}}$ dissoc. time from $\mathrm{RUNX2_{act}}+\mathrm{OSX_{mon}}$ comp.	$T_{\mathrm{RUNX2_{act}}+\mathrm{OSX_{mon}}\rightarrow\mathrm{OSX_{mon}}}$	20	s
$\mathrm{OSX_{mon}}+\mathrm{DNA}$ dissoc. time from $\mathrm{RUNX2_{act}}$	$T_{\mathrm{RUNX2_{act}}+\mathrm{OSX_{mon}}+\mathrm{DNA}\rightarrow\mathrm{OSX_{mon}}+\mathrm{DNA}}$	30	s
$\mathrm{OSX_{mon}}+\mathrm{DNA}$ dissoc. time from AP1	$T_{\mathrm{RUNX2_{act}}+\mathrm{OSX_{mon}}+\mathrm{DNA}+\mathrm{AP1}\rightarrow\mathrm{OSX_{mon}}+\mathrm{DNA}}$	0	s
$\mathrm{OSX_{mul}}$ dissoc. time from $\mathrm{RUNX2_{act}}+\mathrm{OSX_{mul}}$ comp.	$T_{\mathrm{RUNX2_{act}}+\mathrm{OSX_{mul}}\rightarrow\mathrm{OSX_{mul}}}$	40	s
$\mathrm{OSX_{mul}}+\mathrm{DNA}$ dissoc. time from $\mathrm{RUNX2_{act}}$	$T_{\mathrm{RUNX2_{act}}+\mathrm{OSX_{mul}}+\mathrm{DNA}\rightarrow\mathrm{OSX_{mul}}+\mathrm{DNA}}$	50	s
ribosome availability time from $\mathrm{Rib_{n\ av}}+\mathrm{OPN_{RNA}}$	$T_{\mathrm{Rib_{n\ av}}+\mathrm{OPN_{RNA}}\rightarrow\mathrm{Rib_{av}}+\mathrm{OPN_{RNA}}}$	20	s
$\mathrm{OPN_{RNA}}$ dissociation time from available ribosome	$T_{\mathrm{Rib_{av}}+\mathrm{OPN_{RNA}}\rightarrow\mathrm{OPN_{RNA}}}$	75	s
ribosome availability time from $\mathrm{Rib_{n\ av}}+\mathrm{OCN_{RNA}}$	$T_{\mathrm{Rib_{n\ av}}+\mathrm{OCN_{RNA}}\rightarrow\mathrm{Rib_{av}}+\mathrm{OCN_{RNA}}}$	20	s
$\mathrm{OCN_{RNA}}$ dissociation time from available ribosome	$T_{\mathrm{Rib_{av}}+\mathrm{OCN_{RNA}}\rightarrow\mathrm{OCN_{RNA}}}$	75	s
ribosome availability time from $\mathrm{Rib_{n\ av}}+\mathrm{ALP_{RNA}}$	$T_{\mathrm{Rib_{n\ av}}+\mathrm{ALP_{RNA}}\rightarrow\mathrm{Rib_{av}}+\mathrm{ALP_{RNA}}}$	20	s
$\mathrm{ALP_{RNA}}$ dissociation time from available ribosome	$T_{\mathrm{Rib_{av}}+\mathrm{ALP_{RNA}}\rightarrow\mathrm{ALP_{RNA}}}$	75	s
ribosome availability time from $\mathrm{Rib_{n\ av}}+\mathrm{BSP_{RNA}}$	$T_{\mathrm{Rib_{n\ av}}+\mathrm{BSP_{RNA}}\rightarrow\mathrm{Rib_{av}}+\mathrm{BSP_{RNA}}}$	20	s
$\mathrm{BSP_{RNA}}$ dissociation time from available ribosome	$T_{\mathrm{Rib_{av}}+\mathrm{BSP_{RNA}}\rightarrow\mathrm{BSP_{RNA}}}$	75	s
RNA dissociation time from $\mathrm{Rib_{n\ comp}}$	$T_{\mathrm{Rib_{n\ comp}}+\mathrm{RNA}\rightarrow\mathrm{Rib_{n\ comp}}}$	100	s
RNA dissociation time from complete ribosome	$T_{\mathrm{Rib_c}+\mathrm{RNA}\rightarrow\mathrm{Rib_c}}$	100	s
force tag probability	F_{tag}	$P_{\{01,02\}}=\{0.9,0.1\}$	
$\mathrm{I_d}$ interaction radius	$R_{\mathrm{I_d}}$	50	nm
$\mathrm{FAK_{act}}$ interaction radius	$R_{\mathrm{FAK_{act}}}$	50	nm
$\mathrm{RAS_d}$ interaction radius	$R_{\mathrm{RAS_d}}$	80	nm
$\mathrm{RAF_d}$ interaction radius	$R_{\mathrm{RAF_d}}$	70	nm
$\mathrm{MEK_d}$ interaction radius	$R_{\mathrm{MEK_d}}$	50	nm
$\mathrm{ERK_d}$ interaction radius	$R_{\mathrm{ERK_d}}$	30	nm
$\mathrm{RUNX2_d}$ interaction radius	$R_{\mathrm{RUNX2_d}}$	30	nm
$\mathrm{OSX_{mon}}$ interaction radius	$R_{\mathrm{OSX_{mon}}}$	30	nm
$\mathrm{Rib_{n\ comp}}$ interaction radius	$R_{\mathrm{Rib_{n\ comp}}}$	30	nm
cell radius	R_{cell}	1000	nm
nucleus radius	R_{nucl}	400	nm
protein' s average velocity	$\overline{v_p}$	2	nm/s
protein' s velocity variation	$\overline{\Delta v_p}$	1	nm/s
protein' s direction variation	$\overline{\Delta\varphi_p}=\overline{\Delta\theta_p}$	$\pi/10$	rad
protein translation delay	T_p	95	s
transcription delay per mRNA	T_{RNA}	600	s
Integrins θ angle on cell membrane distribution	I_θ	$U[0,\pi]$	1/rad
Integrins ϕ angle on cell membrane distribution	I_ϕ	$U[0,2\pi]$	1/rad

Supplementary table 2: Parameters' name, symbols and values.

Parameter	Symbol	List of values	Unit of measure
Mechanical max. magnitude	M	$\{1000, 10000\}$	μPa
Mechanical period	P	$\{10000, 50000, 2000000\}$	s
$\mathrm{MEK_{act}}$ dissoc. time from $\mathrm{RAF_{act}} + \mathrm{MEK_d}$ comp.	$T_{\mathrm{RAF_{act}}+\mathrm{MEK_d}\rightarrow\mathrm{MEK_{act}}}$	$\{\mathbf{10}, 90, 300, 480, 1320\}$	s
$\mathrm{MEK_{act}}$ dissoc. time from $\mathrm{MEK_{act}} + \mathrm{ERK_d}$ comp.	$T_{\mathrm{MEK_{act}}+\mathrm{ERK_d}\rightarrow\mathrm{MEK_{act}}}$	$\{\mathbf{8}, 90, 300, 480, 1320\}$	s
$\mathrm{MEK_d}$ relaxation time	$T_{\mathrm{MEK_{act}}\rightarrow\mathrm{MEK_d}}$	$\{\mathbf{60}, 90, 300, 480, 1320\}$	s
$\mathrm{ERK_{act}}$ activation time	$T_{\mathrm{MEK_{act}}+\mathrm{ERK_d}\rightarrow\mathrm{ERK_{act}}}$	$\{\mathbf{8}, 90, 300, 480, 1320\}$	s
$\mathrm{ERK_d}$ relaxation time	$T_{\mathrm{ERK_{act}}\rightarrow\mathrm{ERK_d}}$	$\{\mathbf{90}, 300, 480, 600, 1320\}$	s
$\mathrm{ERK_{act}}$ dissoc. time from $\mathrm{ERK_{act}} + \mathrm{RUNX2_d}$ comp.	$T_{\mathrm{ERK_{act}}+\mathrm{RUNX2_d}\rightarrow\mathrm{ERK_{act}}}$	$\{\mathbf{10}, 90, 300, 480, 1320\}$	s

Supplementary table 3: Parameter ranges

Names, symbols, unit of measures and list of values simulated. Bold quantities represent the baseline values. Where no baseline is present, then all possible combinations has been considered. Each set of parameters has been independently repeated 10 times.

FLAME

FLAME, capable of generating C based parallelisable code executable on different parallel hardware architectures, was used to create and simulate the model. FLAME implements a discrete time-fixed sweep update scheme meaning in the simulation, that the time advances at each iteration of a fixed amount defined as time unit in which all agents are updated only once in an internal defined order

References

1. Burge, R., Worley, D., Johansen, A. & Bose, U. THE COST OF OSTEOPOROTIC FRACTURES IN THE UNITED KINGDOM. *Value in Health* **4**, 66-67 (2001).
2. Friedl, P. & Mayor, R. Tuning Collective Cell Migration by Cell–Cell Junction Regulation. *Cold Spring Harbor Perspectives in Biology* **9**(2017).
3. Capulli, M., Paone, R. & Rucci, N. Osteoblast and osteocyte: Games without frontiers. *Archives of Biochemistry and Biophysics* **561**, 3-12 (2014).
4. Mullen, C.A., Haugh, M.G., Schaffler, M.B., Majeska, R.J. & McNamara, L.M. Osteocyte differentiation is regulated by extracellular matrix stiffness and intercellular separation. *Journal of the mechanical behavior of biomedical materials* **28**, 183-194 (2013).
5. Papachroni, K.K., Karatzas, D.N., Papavassiliou, K.A., Basdra, E.K. & Papavassiliou, A.G. Mechanotransduction in osteoblast regulation and bone disease. *Trends in Molecular Medicine* **15**, 208-216 (2009).
6. Batra, N.*, et al.* Mechanical stress-activated integrin α5β1 induces opening of connexin 43 hemichannels. *Proceedings of the National Academy of Sciences* **109**, 3359-3364 (2012).
7. Jiang, P.*, et al.* Load-Induced Modulation of Signal Transduction Networks. *Science Signaling* **4**, ra67-ra67 (2011).
8. Shuaib, A., et al. Heterogeneity in The Mechanical Properties of Integrins Determines Mechanotransduction Dynamics in Bone Osteoblasts. Scientific reports 9, 13113-13113 (2019).
9. Sun, Z., Guo, S.S. & Fässler, R. Integrin-mediated mechanotransduction. *The Journal of Cell Biology* **215**, 445 (2016).
10. Liu, L.*, et al.* The interaction between β1 integrins and ERK1/2 in osteogenic differentiation of human mesenchymal stem cells under fluid shear stress modelled by a perfusion system. *Journal of Tissue Engineering and Regenerative Medicine* **8**, 85-96 (2014).
11. Yang, J.M.*, et al.* Integrating chemical and mechanical signals through dynamic coupling between cellular protrusions and pulsed ERK activation. *Nat Commun* **9**, 4673 (2018).
12. Hirano, T.*, et al.* Anabolic effects of human biosynthetic parathyroid hormone fragment (1-34), LY333334, on remodeling and mechanical properties of cortical bone in rabbits. *J Bone Miner Res* **14**, 536-545 (1999).
13. Kim, C.H.*, et al.* Trabecular bone response to mechanical and parathyroid hormone stimulation: the role of mechanical microenvironment. *J Bone Miner Res* **18**, 2116-2125 (2003).
14. Alonso, J.L. & Goldmann, W.H. Cellular mechanotransduction. *transport* **1**, 7 (2016).
15. Harris, A.R., Jreij, P. & Fletcher, D.A. Mechanotransduction by the Actin Cytoskeleton: Converting Mechanical Stimuli into Biochemical Signals. *Annual Review of Biophysics* **47**, 617-631 (2016).
16. Martino, F., Perestrelo, A.R., Vinarský, V., Pagliari, S. & Forte, G. Cellular Mechanotransduction: From Tension to Function. *Frontiers in Physiology* **9**(2018).
17. Yap, A.S., Duszyc, K. & Viasnoff, V. Mechanosensing and Mechanotransduction at Cell–Cell Junctions. *Cold Spring Harbor Perspectives in Biology* **10**(2018).
18. Humphrey, J.D., Dufresne, E.R. & Schwartz, M.A. Mechanotransduction and extracellular matrix homeostasis. *Nature Reviews Molecular Cell Biology* **15**, 802 (2014).
19. Vincent, T.L. Targeting mechanotransduction pathways in osteoarthritis: a focus on the pericellular matrix. *Current Opinion in Pharmacology* **13**, 449-454 (2013).
20. Klein-Nulend, J., Bacabac, R.G., Veldhuijzen, J.P. & Van Loon, J.J. Microgravity and bone cell mechanosensitivity. *Advances in space research : the official journal of the Committee on Space Research (COSPAR)* **32**, 1551-1559 (2003).
21. Tatsumi, S.*, et al.* Targeted ablation of osteocytes induces osteoporosis with defective mechanotransduction. *Cell metabolism* **5**, 464-475 (2007).

22. Shuaib, A., Hartwell, A., Kiss-Toth, E. & Holcombe, M. Multi-Compartmentalisation in the MAPK Signalling Pathway Contributes to the Emergence of Oscillatory Behaviour and to Ultrasensitivity. *PLOS ONE* **11**, e0156139 (2016).
23. Fujioka, A.*, et al.* Dynamics of the Ras/ERK MAPK Cascade as Monitored by Fluorescent Probes. *Journal of Biological Chemistry* **281**, 8917-8926 (2006).
24. Legewie, S., Schoeberl, B., Blüthgen, N. & Herzel, H. Competing docking interactions can bring about bistability in the MAPK cascade. *Biophys J* **93**, 2279-2288 (2007).
25. Rhodes, D.M., Holcombe, M. & Qwarnstrom, E.E. Reducing complexity in an agent based reaction model—Benefits and limitations of simplifications in relation to run time and system level output. *Biosystems* **147**, 21-27 (2016).
26. Gorenflo, R. & Mainardi, F. Subordination pathways to fractional diffusion. *The European Physical Journal Special Topics* **193**, 119-132 (2011).
27. Sokolov, I.M. & Klafter, J. From diffusion to anomalous diffusion: A century after Einstein's Brownian motion. *Chaos: An Interdisciplinary Journal of Nonlinear Science* **15**, 026103 (2005).
28. Schneider, G.B., Zaharias, R. & Stanford, C. Osteoblast integrin adhesion and signaling regulate mineralization. *J Dent Res* **80**, 1540-1544 (2001).
29. Shekaran, A.*, et al.* The effect of conditional inactivation of beta 1 integrins using twist 2 Cre, Osterix Cre and osteocalcin Cre lines on skeletal phenotype. *Bone* **68**, 131-141 (2014).
30. Fullstone, G., Wood, J., Holcombe, M. & Battaglia, G. Modelling the Transport of Nanoparticles under Blood Flow using an Agent-based Approach. *Scientific reports* **5**, 10649 (2015).
31. Pogson, M., Holcombe, M., Smallwood, R. & Qwarnstrom, E. Introducing Spatial Information into Predictive NF-κB Modelling – An Agent-Based Approach. *PLOS ONE* **3**, e2367 (2008).
32. Pogson, M., Smallwood, R., Qwarnstrom, E. & Holcombe, M. Formal agent-based modelling of intracellular chemical interactions. *Biosystems* **85**, 37-45 (2006).
33. Richmond, P., Walker, D., Coakley, S. & Romano, D. High performance cellular level agent-based simulation with FLAME for the GPU. *Briefings in Bioinformatics* **11**, 334-347 (2010).
34. Ascolani, G., Skerry, T.M., Lacroix, D., Dall'Ara, E. & Shuaib, A. Revealing hidden information in osteoblast's mechanotransduction through analysis of time patterns of critical events. BMC Bioinformatics 21, 114 (2020).
35. Khatiwala, C.B., Kim, P.D., Peyton, S.R. & Putnam, A.J. ECM compliance regulates osteogenesis by influencing MAPK signaling downstream of RhoA and ROCK. *J Bone Miner Res* **24**, 886-898 (2009).
36. Tomida, T., Takekawa, M. & Saito, H. Oscillation of p38 activity controls efficient pro-inflammatory gene expression. *Nature Communications* **6**, 8350 (2015).
37. Albeck, John G., Mills, Gordon B. & Brugge, Joan S. Frequency-Modulated Pulses of ERK Activity Transmit Quantitative Proliferation Signals. *Molecular Cell* **49**, 249-261 (2013).
38. Aoki, K.*, et al.* Stochastic ERK Activation Induced by Noise and Cell-to-Cell Propagation Regulates Cell Density-Dependent Proliferation. *Molecular Cell* **52**, 529-540 (2013).
39. Waters, K.M., Cummings, B.S., Shankaran, H., Scholpa, N.E. & Weber, T.J. ERK oscillation-dependent gene expression patterns and deregulation by stress response. *Chem Res Toxicol* **27**, 1496-1503 (2014).
40. Simpson, M.L.*, et al.* Noise in biological circuits. *Wiley interdisciplinary reviews. Nanomedicine and nanobiotechnology* **1**, 214-225 (2009).
41. Tian, T. & Harding, A. How MAP kinase modules function as robust, yet adaptable, circuits. *Cell cycle (Georgetown, Tex.)* **13**, 2379-2390 (2014).
42. Mogil, R.J.*, et al.* Effect of Low-Magnitude, High-Frequency Mechanical Stimulation on BMD Among Young Childhood Cancer Survivors: A Randomized Clinical Trial. *JAMA oncology* **2**, 908-914 (2016).

43. Nakai, N.*, et al.* Mechanical stretch activates signaling events for protein translation initiation and elongation in C2C12 myoblasts. *Molecules and Cells* **30**, 513-518 (2010).
44. Gesty-Palmer, D.*, et al.* A β-Arrestin–Biased Agonist of the Parathyroid Hormone Receptor (PTH1R) Promotes Bone Formation Independent of G Protein Activation. *Science Translational Medicine* **1**, 1ra1 (2009).
45. Gesty-Palmer, D. & Luttrell, L.M. 'Biasing' the parathyroid hormone receptor: A novel anabolic approach to increasing bone mass? *British Journal of Pharmacology* **164**, 59-67 (2011).
46. Yavropoulou, M.P. & Yovos, J.G. The molecular basis of bone mechanotransduction. *Journal of musculoskeletal & neuronal interactions* **16**, 221-236 (2016).
47. Arkin, M.R., Tang, Y. & Wells, J.A. Small-molecule inhibitors of protein-protein interactions: progressing toward the reality. *Chem Biol* **21**, 1102-1114 (2014).
48. Rudin, C.M.*, et al.* Phase II study of single-agent navitoclax (ABT-263) and biomarker correlates in patients with relapsed small cell lung cancer. *Clin Cancer Res* **18**, 3163-3169 (2012).
49. Vassilev, L.T.*, et al.* In vivo activation of the p53 pathway by small-molecule antagonists of MDM2. *Science (New York, N.Y.)* **303**, 844-848 (2004).